Interfacial structure of two-dimensional epitaxial Er silicide on Si(111)

M. H. Tuilier, P. Wetzel, C. Pirri, D. Bolmont, and G. Gewinner
Laboratoire de Physique et Spectroscopie Electronique, Faculté des Sciences et Techniques, 4, rue des Frères Lumière, 68093 Mulhouse Cédex France
(Received 28 January 1994)

Auger-electron diffraction (AED) and surface-extended x-ray-absorption fine structure (SEXAFS) have been used to obtain a complete description of the atomic structure of a two-dimensional epitaxial Er silicide layer on Si(111). AED reveals that a monolayer of Er is located underneath a buckled Si double layer. The relevant Er-Si interlayer spacings are determined by means of single scattering cluster simulations and a R-factor analysis to be 1.92 ± 0.05 Å to the first and 2.70 ± 0.05 Å to the second Si top layer. Er near-neighbor bond lengths and coordination numbers are obtained independently from polarization-dependent SEXAFS. The SEXAFS data, when combined with the Si top-layer geometry inferred from AED, permit the determination of the atomic positions at the silicide/Si(111) interface. The Er is found to reside in relaxed T_4 sites of Si(111) with a single Er-Si distance of 3.09 ± 0.04 Å to the first- and second-layer Si atoms of the substrate.

I. INTRODUCTION

Epitaxial metal-semiconductor interfaces are of great interest for investigating the physics involved in the Schottky barriers formed at such contacts. More generally, they are very attractive not only to test first-principles calculations but also to unravel the causal relationships between the geometric and electronic structures of well-ordered crystalline interfaces. Unfortunately, the atomic geometry has been determined experimentally only for very few interfaces. An example of a epitaxial metal-semiconductor interface with a good degree of perfection is $NiSi_2$/Si(111). Two types of distinct interface structures labeled A (same orientation) and B (180° rotated) have been identified experimentally,[1,2] and their atomic geometry studied by different techniques.[1,3–5] Interestingly these two interfaces show Schottky-barrier heights differing by ~ 0.14 eV.[6,7] The screened charge transfer across the interface, which determines the observed Schottky barrier, obviously depends on details in the interface structure.[8,9] Among other promising model systems well adapted to the investigation of interface properties, rare-earth silicides appear to be particularly interesting. First, they form unusually low barriers with n-type silicon ($E_B \sim 0.30$ eV), indicating that they behave in a peculiar way when compared with classical metal-semiconductor interfaces like Au-Si, where the Fermi level is pinned near midgap. Second, they can be grown epitaxially on Si(111) with good structural perfection.[10–13]

The purpose of this paper is to shed more light on the interfacial structure of a rare-earth silicide, namely Er disilicide on Si(111). $ErSi_{2-x}$ crystallizes in the AlB_2-type structure with defects in the Si lattice and a stoichiometry close to $x=0.33$. In epitaxial films $ErSi_{2-x}(0001)$ is parallel to Si(111), and a $\sqrt{3}\times\sqrt{3}\ R30°$ superstructure is observed and commonly attributed to ordered arrays of Si vacancies.[11] To determine the atomic structure of a buried interface is a difficult problem. Hence in this work we concentrate on the atomic geometry of a single Er silicide layer grown epitaxially on Si(111). Standard surface-structure-sensitive techniques can effectively be utilized for the study of such a system. As shown in previous work,[14,15] this silicide layer can readily be prepared with a very high degree of crystallinity by annealing one Er monolayer (ML) deposited on Si(111) at room temperature. Though this interface closely resembles the interfaces obtained with thicker $ErSi_{2-x}$ layers and much may be learned on the latter technologically more important systems from the present study, there are some remarkable differences. First, the silicide monolayer exhibits a p (1×1) pattern as opposed to the $\sqrt{3}\times\sqrt{3}R30°$ superstructure observed on thicker layers by low-energy electron diffraction (LEED), i.e. there is no evidence of Si vacancies and related defects. Second, the single-layer silicide forms an even lower Schottky barrier with n-type silicon than thicker layers. Our measurements based on photoemission indicate barrier heights $E_B \simeq 0.10$ eV or less,[16] i.e., the Fermi level moves very close to the conduction-band edge upon formation of the interface. Third, valence-band photoemission studies reveal that the electronic structure characteristic of thick epitaxial $ErSi_{2-x}$ layers is fully developed only for layer thicknesses larger than ~ 20 silicide layers,[17] though the Schottky-barrier height of buried interfaces ($E_B \simeq 0.30$ eV) is already observed for thicknesses as small as ~ 2 silicide layers.[16,18] It is clear that the extremely low barrier to n-type Si doping, the very good structural perfection, and the simple (1×1) translation symmetry without Si vacancies and related defects makes the single $ErSi_2$ layer on Si(111) very attractive for model case studies of epitaxial metal-semiconductor interfaces. Here we combine Auger-electron diffraction (AED) and surface-extended x-ray-absorption fine structure (SEXAFS) to determine completely the structure and particularly the bonding geometry at the interface for this system. Both techniques are based on the observation of interferences between the direct Auger or photoelectron wave emitted by a specific atom and those scat-

tered by the strong core potential of atoms neighboring the emitter. In AED, the intensity of the Er *MNN* Auger line at 1430 eV is measured as a function of polar angle of emission along selected azimuths. At these high kinetic energies the observed modulations in intensity show conspicuous peaks due to forward focusing[19,20] along bond directions to nearest neighbors. More generally, only small-angle ($\leq 50°$) scattering events involving scatterers relatively close to the emitter-detector direction effectively contribute to the structure observed in the polar intensity profiles. Hence AED profiles give specific structural information about those neighbors located *above* the Er plane, and the high directionality of the elastic-scattering cross section emphasizes zero-order interference and *bond directions*. In contrast, in SEXAFS, where the modulations in the x-ray absorption are measured versus photon energy at the Er L_3 edge, the relevant interferences take place between the direct photoelectron wave and those waves backscattered by neighboring atoms to the emitter.[21] The SEXAFS data therefore reflect large-angle (180°) scattering events and are more sensitive to *bond lengths* and coordination numbers than bond directions. In particular, SEXAFS probes the bonds to the neighbors located both *above and below* the Er plane. Both techniques are quite complementary, the knowledge of the top-layer structure gained from AED allowing a detailed interpretation of the polarization-dependent SEXAFS data and the determination of the silicide-silicon interfacial structure.

II. EXPERIMENT

Single-layer silicide films were prepared in the same way for AED and SEXAFS measurements in UHV chambers equipped with Er sources, sample heating and cleaning facilities, quartz-crystal microbalances, and LEED optics. The Er was evaporated onto clean Si(111) 7×7 at a rate of about 0.5 monolayer (ML)/min and a base pressure below 2.10^{-10} Torr. The monolayer scale is referred to the density of Si on the ideal Si(111) surface. As shown in previous work,[14,15] annealing at 400 °C of Er amounts in the submonolayer range results in single-layer two-dimensional $ErSi_2$ islands that eventually cover the whole surface for a 1-ML Er deposit. The two-dimensional silicide is characterized by a very sharp low background $p(1\times1)$ LEED pattern with a marked threefold symmetry as well as characteristic valence-band photoemission features.[22] In all measurements presented here, care was taken during sample preparation not to exceed the nominal 1-ML Er deposit and form a second silicide layer. This is checked by the absence of the characteristic $\sqrt{3}\times\sqrt{3}R\,30°$ superstructure as well as the definitely different valence-band photoemission signature observed for thicknesses larger than 1 ML. The experimental setup used for the AED measurements consists of a Leybold Heraeus EA 200 electron spectrometer. The two-stage electron lens at the entry of the energy analyzer was operated at an angular resolution of $\pm1°$. Unpolarized Al $K\alpha$ radiation from a high-power (1600 W) x-ray source was used to excite the Er *MNN* Auger line at a kinetic energy of 1430 eV. The relevant electrons were analyzed with a large hemispherical energy analyzer, 150 mm in radius, and a multichannel detector. In this way very good counting statistics were obtained at the highest $\pm1°$ angular resolution. The polar angle Θ of the electron emission direction was scanned by rotating the sample in a fixed excitation-analyzer geometry. Three azimuthal orientations along the inequivalent high-symmetry $[\bar{1}01]$, $[\bar{1}2\bar{1}]$, and $[1\bar{2}1]$ directions of the Si(111) plane were investigated.

The SEXAFS data were recorded on the ErL_3 edge (8347 eV) using the x rays supplied by the wiggler beam line of the DCI storage ring at the Laboratoire pour l'Utilisation du Rayonnement Electromagnétique (LURE, Orsay France). The harmonics were rejected at the entrance of the beamline using a curved mirror at 1-mrad incidence. The white radiation was monochromatized by a Si(311) two-crystal monochromator. The SEXAFS UHV chamber includes a sample manipulator that allows sample rotation around the vertical direction, so that the angle of incidence of the x rays can be varied. The Er L_3-edge SEXAFS data were collected at room temperature by measuring the total electron yield with a channeltron at three different angles ψ between the electric field or polarization vector of the synchrotron radiation and the normal to the sample: glancing incidence ($\psi=15°$), magic angle ($\psi=55°$), and normal incidence ($\psi=90°$).

Data about standard compounds were also obtained, in the same collection mode, from a 200-Å-thick $ErSi_{1.7}$ sample grown epitaxially on Si(111). EXAFS spectra of powdered $ErSi_{1.7}$ were collected by transmission detection at Er L_3 and L_1 edges in a different experimental setup. Details about epitaxial and powdered $ErSi_{1.7}$ are given in Refs. 18 and 23, respectively.

III. AED RESULTS AND DATA ANALYSIS

The Er *MNN* Auger intensity measured as a function of polar angle along the opposite $[\bar{1}2\bar{1}]$ and $[1\bar{2}1]$ azimuths is shown in Fig. 1. Along the $[\bar{1}01]$ azimuth the polar profile (not shown) is found to be essentially featureless, and reflects the instrumental response function. In agreement with LEED, the AED data exhibit a remarkable 3-m point-group symmetry that results in definitely different polar profiles along the opposite $[\bar{1}2\bar{1}]$ and $[1\bar{2}1]$ azimuths. As pointed out in Sec. I, the structure observed in AED at a kinetic energy of 1430 eV is due to scattering at atoms located above the Er emitter. There is no sensitivity to the structure at the Er-Si substrate interface because of the strongly forward-peaked scattered amplitude at high kinetic energies (≥ 500 eV). Scattering of the Er emission by substrate Si atoms (located below the Er emitter) into the detector involves large scattering angles and thus very small scattered amplitudes. In a preliminary analysis of similar data based on such forward-focusing considerations,[15] we arrived at the conclusion that Er forms an ordered hexagonal monolayer accommodated underneath a buckled Si top layer similar to Si(111) double layers in Si bulk. The relevant structural model is depicted in Fig. 2. We concentrate here on the top-layer geometry that can be derived sim-

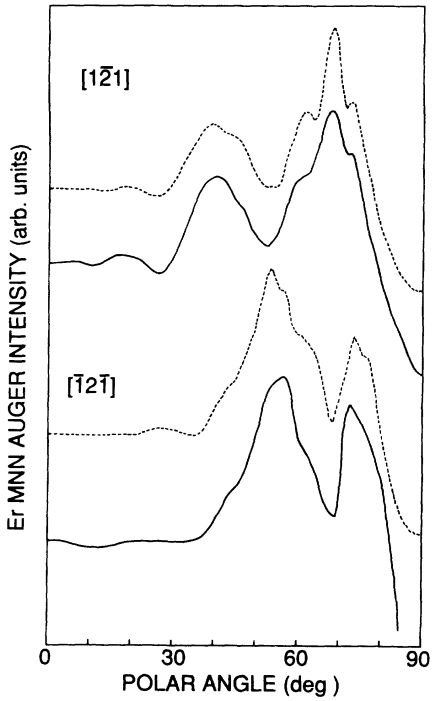

FIG. 1. Experimental (solid lines) and theoretical (dashed lines) Er *MNN* Auger electron polar intensity profiles along the [$\bar{1}$2$\bar{1}$] and [1$\bar{2}$1] azimuths for a single $ErSi_2$ layer epitaxially grown on Si(111). The calculated profiles correspond to the best-fit atomic structure.

ply from a single $ErSi_2$ layer with AlB_2-type structure by moving upwards every second Si atom in the top Si(0001) plane. It was also shown in Ref. 15 that only domains of *B*-type orientation are actually formed, i.e., the buckled Si top layer is always rotated by 180° around surface normal with respect to the relevant Si(111) double layers in the Si substrate. This atomic configuration is consistent with the observed threefold symmetry (as opposed to the sixfold symmetry of the ideal AlB_2 structure) as well as the absence of any significant modulation in the polar profile along the [$\bar{1}$01] azimuth. In contrast, the strong forward-focusing peaks, as well as specific fine structure along [$\bar{1}$2$\bar{1}$] and [1$\bar{2}$1] azimuths, reflect the scattering of the Er *MNN* Auger electrons at the two types of Si atoms in the buckled Si top layer, namely Si_{down} and Si_{up}. For instance, the prominent feature along [1$\bar{2}$1] near 40° is due mainly to forward focusing along the Er-Si_{up} bond axis. The relevant Er-Si interlayer distances $d_1(Si_{down})$ and $d_2(Si_{up})$ were estimated in Ref. 15 by simple triangulation and visual comparison of the experimental profiles with single-scattering plane-wave simulations. Here we present a more refined analysis of the AED data in order to determine with better accuracy these interlayer spacings used as an input in the analysis of the SEXAFS data presented in Sec. IV. The experiment is compared by means of a reliability factor (*R*-factor) analysis to calculated profiles for a set of d_1 and d_2 values. The calculations are conducted using a single-scattering spherical wave cluster approximation.[24] The primary Auger wave is taken to be an *s* wave. Multiple scattering is not expected to give sizable effects in the present ultrathin layer geometry except at large ($\geq 80°$) polar angles, i.e., grazing emission,[25] where the small instrumental response limits the collection of experimental data. A cluster, about 20 Å in radius, containing as many as 200 atoms is found to be necessary in order to reproduce the observed fine structure in the profiles. This fine structure is generally observed at high angular resolution superimposed on the strong and broader forward scattering peaks due to focusing by nearest or next-nearest neighbors.[26] It results from scattering at more distant atoms (up to ~20 Å from the emitter), which make a sizable contribution at polar angles $\Theta \geq 40°$ in the present monolayer configuration.

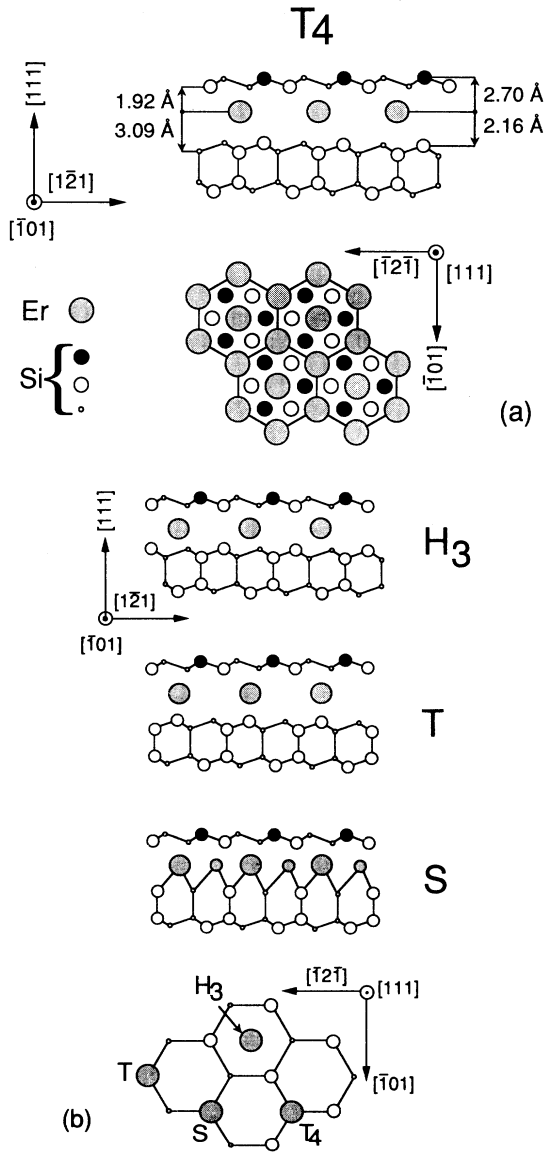

FIG. 2. (a) Top and side views of the atomic structure of a single $ErSi_2$ layer epitaxially grown on Si(111), with the optimized parameters deduced from this work. The Er is found to reside in relaxed T_4 sites, i.e., eclipsed threefold hollows of the substrate. (b) Other possible atomic geometries at the interface namely substitutional (*S*), top (*T*), and threefold hollow (H_3) tested in this work.

On the other hand, by test calculations we have checked that, as expected, substrate Si atoms do not contribute significantly to the modulations and can be ignored in the simulations. Figure 3 shows how the R factor based on a normalized absolute deviation between experimental and theoretical profiles along $[\bar{1}2\bar{1}]$, $[1\bar{2}1]$, and $[\bar{1}01]$ azimuths varies as Er-Si layer spacings d_1 and d_2 are changed. As can be seen, there is only one well-defined minimum in the parameter space investigated, and the best fit is obtained for $d_1 = 1.92 \pm 0.05$ Å and $d_2 = 2.70 \pm 0.05$ Å. The quoted errors mainly reflect the changes in the location of the minimum when different R factors are used. In Fig. 1 we compare the calculated profiles for the optimized geometry with experiment, and show the level of visual agreement obtained in this study.

IV. SEXAFS RESULTS AND DATA ANALYSIS

Figure 4 shows the raw $k\chi(k)ErL_3$ SEXAFS data recorded from a single Er disilicide layer (1-ML coverage) at normal [Fig. 4(a)], magic [Fig. 4(b)], and glancing [Fig. 4(c)] incidences. The curves display the data following normalization to unit step edge height, background removal, and conversion to k space using the standard procedure.[27] The raw data are shown together with their first-shell Fourier-filtered contribution. The Fourier transforms (FT) of $k^2\chi(k)$ data between 2.3 and 9.5 Å^{-1} are shown in Fig. 5. The strong polarization dependence of the SEXAFS data is confirmed on FT. The peak observed below 2 Å in FT is due to long-wavelength oscillations of the atomic absorption coefficient and has no structural meaning. The peak around 2.5 Å, which corresponds to the first silicon neighbors of erbium, is asymmetrical and its maximum is shifted toward higher coordination radii upon decreasing the polarization angle ψ [Figs. 5(b) and 5(c)]. A further peak near 3.6 Å is related to the nearest Er neighbors in the hexagonal Er atomic plane. This peak becomes very weak at grazing incidence because it corresponds to Er-Er interatomic bonds parallel to the surface. When corrected for the scattering phase shift at the Er atoms, the Er-Er distance is found to

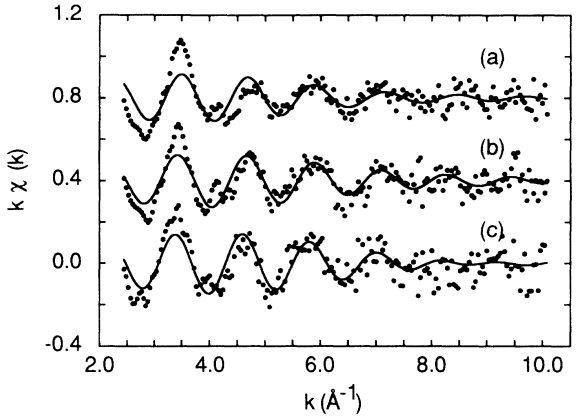

FIG. 4. Raw k-weighted Er L_3 SEXAFS data (dots) recorded from the single $ErSi_2$ layer epitaxially grown on Si(111) in (a) normal incidence ($\psi = 90°$), (b) magic angle ($\psi = 55°$), and (c) glancing incidence ($\psi = 15°$). The data are plotted with their Fourier-filtered first shell contribution.

be 3.84 Å, in excellent agreement with the value expected for strained epitaxial silicide on Si(111). A similar result was obtained for thick epitaxial $ErSi_{2-x}$ layers on Si(111).[28]

Let us now concentrate on the analysis of the first Si neighbor's shell. The Fourier-filtered first shell contribution has been analyzed using single-scattering formalism. The backscattering phase $\phi(k)$ and amplitude $f(k)$ functions have been extracted from the $ErSi_{2-x}$ compound. The complete EXAFS analysis of $ErSi_{2-x}$ is described elsewhere.[28] At this stage we know from LEED and AED measurements that the surface arrangement consists of a hexagonal erbium monolayer and a buckled Si top layer characterized by $d_2 = 2.70 \pm 0.05$ Å and $d_1 = 1.92 \pm 0.05$ Å. The Er-Si bond lengths deduced from this geometry are 3.5 ± 0.05 and 2.93 ± 0.05 Å, respectively. Only the three silicon atoms lying at the shorter distance contribute to the first-neighbor shell. On the other hand, below the erbium atomic plane four possible interfacial geometries may be considered, namely H_3, S, T and

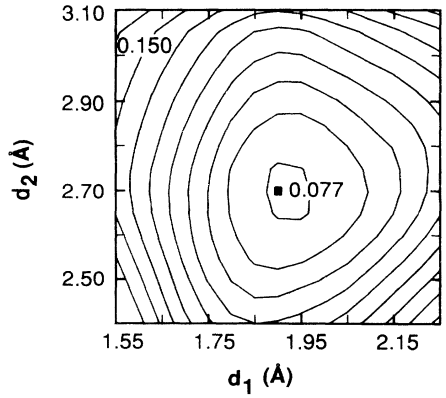

FIG. 3. Dependence of the R factor (namely R_1, which sums the normalized absolute deviations between experiment and theory) on the Er-Si top-layer spacings d_1 and d_2 in the form of a contour map.

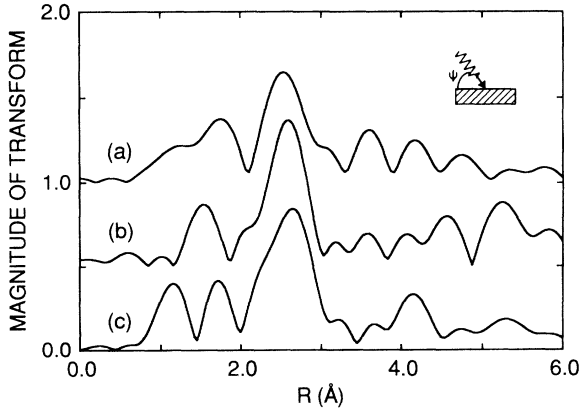

FIG. 5. k^2-weighted Fourier transforms of SEXAFS data presented in Fig. 4. The polarization angles ψ are (a) 90°, (b) 55°, and (c) 15°.

T_4. The relevant bonding configurations are shown in Fig. 2. In H_3 and T_4 geometries, Er occupies respectively threefold and eclipsed threefold hollow sites of the Si(111) substrate termination. The S (T) sites are substitutional (top) sites where the Er replaces (is located just above) the Si atoms in the top layer of the substrate. In H_3 and S geometries the erbium atoms have a similar first coordination shell with three nearest Si neighbors in the substrate. The difference between the H_3 and S sites is only reflected in the second coordination shells. Erbium placed in T and T_4 sites has one and four Si neighbors in the substrate, respectively. Thus the possible first shell coordination numbers of erbium in the thin film are 6 (H_3 or S), 4 (T), and 7 (T_4).

The simulation of the Fourier-filtered first shell SEXAFS data recorded at the "magic" angle gives a value of 2.99 Å for the average Er-Si bond length $R_{\text{Er-Si}}$. The results of the simulations are summarized in Table I. The rather large values of $R_{\text{Er-Si}}$ and the Debye-Waller factor σ indicate a contribution of silicon neighbors at a distance larger than 2.93 Å, the Er-Si bond length in the top layer being inferred from AED. The same treatment of the data recorded at normal and grazing incidences shows an increase of $R_{\text{Er-Si}}$ as ψ decreases. This evolution is quite inconsistent with the roughly isotropic Si neighbors contribution expected for H_3 or S geometries. In contrast, it is the expected behavior in T and T_4 models, where Er occupies atop positions of the Si substrate with Er-Si bonds along the surface normal that contribute strongly to the EXAFS signal when the electric field vector has a sizable projection along the surface normal. Since the results of AED allow us to rule out the presence of perpendicular Er-Si bonds above the erbium atomic plane, this kind of bond must exist at the silicide-substrate interface. However, as can be seen in Table I, the Er-Si coordination radii and numbers are much too large to be consistent with the onefold T geometry. Thus we are left with the fourfold coordinated T_4 geometry as the most probable one for the structure at the interface with the Si(111) substrate.

In order to confirm this geometry, we have considered a better model of the SEXAFS data that assumes a two-component fit with dual near-neighbor bond lengths. In this refined analysis the Fourier-filtered first shell recorded at normal incidence is fairly well accounted for by two Er-Si distances of 2.94 and 3.10 Å, respectively. The first is attributed to the silicon neighbors of Er in the Si top layer, in excellent agreement with AED results. The second is assigned to silicon neighbors at the interface with the substrate. The expected effective coordination numbers N_i^* are first calculated using the formula currently used for L_2 and L_3 edges[29] with a structure that corresponds to d_1 and d_2 values deduced from AED and an Er-Si distance at the interface of 3.10 Å. These values of N^*, which are summarized in Table I for all models investigated, are then used as initial parameters in the simulations. As can be seen in Table I, the results of these refinements for both normal and grazing incidence data are in good agreement with a T_4 geometry, with four silicon neighbors at 3.09±0.04 Å below the erbium atoms. In contrast, other models tested can safely be ruled out on the basis of the present data.

TABLE I. Structural parameters determined from the polarization-dependent SEXAFS analysis of Er L_3 data for the first silicon neighbors of erbium in a single $ErSi_2$ layer epitaxially grown on Si(111). The effective coordination neighbors calculated in the various models described in the text are given in the last three columns.

					Calculated N^*		
ψ	N^*	R (Å)	σ (Å)	Resid.	$T4$	$H3$ or S	T
55°	7	2.99	0.12	0.001	7	6	4
90°	6.4	2.98	0.13	0.015	6.4	5.7	3.6
90°	3.0	2.94	0.08	0.004	2.9	2.9	2.9
	4.0	3.10	0.11	0.004	3.5	2.8	0.7
15°	8.7	3.04	0.13	0.010	8.1	6.6	4.7
15°	3.5	2.94	0.10	0.005	3.3	3.3	3.3
	5.5	3.09	0.09	0.005	4.9	3.3	1.5

V. CONCLUDING REMARKS

Upon combining two surface-structure-sensitive techniques, we have been able to determine the atomic geometry of an Er disilicide monolayer epitaxially grown on Si(111). The Er is located below a Si(111) double layer with a buckling of 0.78 Å similar to the one observed in bulk Si. The Er-Si bond length to the top-layer Si is 2.94 Å, i.e., very close to the mean near-neighbor distance of 2.95 Å measured on bulk $ErSi_{2-x}$ silicide.[28] Nevertheless the Er-Si interlayer distance $d_1=1.92$ Å is contracted with respect to the relevant interlayer distance of 2.01 Å measured by x-ray diffraction in thick Er silicide epilayers.[30] As pointed out in Ref. 28, the mean near-neighbor bond length in bulk $ErSi_{2-x}$ is shorter than expected for the ideal AlB_2 structure (3.00 Å), because of a relaxation of the Si sublattice due to the presence of Si vacancies. For a monolayer of silicide we find that Er occupies T_4 sites of the Si(111) substrate. The polarization-dependent SEXAFS data are quite well simulated with a single Er-Si bond length to the four Si neighbors in the substrate. Thus, within experimental accuracy, the same Er-Si near-neighbor distance is found: 3.09±0.04 Å to the first- and second-layer Si atoms of the substrate. First, this implies an increased buckling of the Si(111) double layer at the substrate-silicide interface by about 0.15 Å. Second, from these bond lengths we deduce an Er-Si interlayer distance of 2.16 Å at the interface, i.e., a relaxation of +0.15 Å with respect to the distance measured in bulk $ErSi_{2-x}$. The fact that Er resides in relaxed T_4 sites is quite consistent with recent work on the electronic structure of such monolayer films.[31] In this study the two-dimensional band dispersions were determined by angle-resolved photoemission and compared with theoretical calculations for different interfacial geometries. For the B-type silicide, actually observed experimentally, only the T_4 geometry resulted in good agreement as to the band topology and location between theory and experiment. The present finding also confirms

the now recognized fact that the T_4 site is a ubiquitous building block for the metal (or vacuum) Si(111) and Ge(111) interfaces.[32] From a theoretical point of view, the T_4 site allows for a better overlap between adsorbate and surface dangling-bond charge density, and results in less induced local strain than the H_3 site.[33–35] Theory also predicts a sizable relaxation of the substrate[32] similar to, but generally larger than, the one observed here. Finally, let us note that this relaxation gives more *s* character to the substrate Si dangling bonds, which are thought to pin the Fermi level after interaction with the silicide. This in turn may favor a large charge transfer from Er to Si and thus a low Schottky barrier to *n*-type silicon.[8]

ACKNOWLEDGMENTS

We are grateful to D. Chandesris, H. Magnan, O. Heckmann, and D. Ragonnet for their assistance during the SEXAFS experiments at the LURE French synchrotron radiation facility. The Laboratoire pour l'Utilisation du Rayonnement Electromagnétique is a Laboratoire du Centre National de la Recherche Scientifique, du Commissariat à l'Energie Atomique et du Ministère de l'Enseignement Supérieur et de la Recherche. The Laboratoire de Physique et de Spectroscopie Electronique is a Laboratoire associé au Centre National de la Recherche Scientifique.

[1] D. Cherns, G. R. Anstis, J. L. Hutchinson, and J. C. H. Spence, Philos. Mag. A **46**, 849 (1982).

[2] J. M. Gibson, R. T. Tung, and J. M. Poate, in *Defects in Semiconductors II,* edited by S. Mahajan and J. W. Corbett, MRS Symposia Proceedings No. 14 (Materials Research Society, Pittsburgh, 1983), p. 395.

[3] E. J. Van Loenen, J. W. M. Frenken, J. F. Van der Veen, B. N. Dev, and S. Valeri, Phys. Rev. Lett. **54**, 827 (1985).

[4] E. Vlieg, A. E. M. Fischer, J. F. Van der Veen, B. N. Dev, and G. Materlik, Surf. Sci. **178**, 36 (1986).

[5] J. Vrijmoeth, J. F. Van der Veen, D. R. Heslinga, and T. M. Klapwijk, Phys. Rev. B **42**, 9598 (1990).

[6] R. T. Tung, Phys. Rev. Lett. **52**, 461 (1984).

[7] R. J. Hauenstein, T. E. Schlesinger, T. E. McGill, B. D. Hunt, and L. J. Schowalter, Appl. Phys. Lett. **47**, 853 (1985).

[8] M. Lannoo and P. Friedel, in *Atomic and Electronic Structure of Surfaces, Theoretical Foundations,* edited by M. Cardona (Springer-Verlag, Berlin, 1991).

[9] W. Mönch, in *Semiconductor Surfaces and Interfaces,* edited by G. Erth (Springer-Verlag, Berlin, 1993).

[10] J. A. Knapp and S. T. Picraux, Appl. Phys. Lett. **48**, 466 (1986).

[11] F. A. d'Avitaya, A. Perio, J. C. Oberlin, V. Campidelli, and J. H. Chroboczek, Appl. Phys. Lett. **54**, 2198 (1989).

[12] F. H. Kaatz, M. P. Siegal, W. R. Graham, J. Van der Spiegel, and J. J. Santiago, Thin Solid Films **184**, 325 (1990).

[13] K. N. Tu, R. D. Thompson, and B. Y. Tsaur, Appl. Phys. Lett. **38**, 626 (1981).

[14] P. Paki, U. Kafader, P. Wetzel, C. Pirri, J. C. Peruchetti, D. Bolmont, and G. Gewinner, Phys. Rev. B **45**, 8490 (1992).

[15] P. Wetzel, C. Pirri, P. Paki, D. Bolmont, and G. Gewinner, Phys. Rev. B **47**, 3677 (1993).

[16] M. H. Tuilier, G. Gewinner, C. Pirri, P. Wetzel, D. Bolmont, and O. Heckmann, European Symposium on Frontiers in Science and Technology with Synchrotron Radiation, Aixen Provence (F), 1994 [J. Phys. (Paris) (to be published)].

[17] P. Wetzel, C. Pirri, D. Bolmont, and G. Gewinner (unpublished).

[18] J. Y. Veuillen, D. B. B. Lollman, T. A. Nguyen Tan, and L. Magaud, Appl. Surf. Sci. **65/66**, 712 (1993).

[19] C. S. Fadley, Prog. Surf. Sci. **16**, 275 (1984).

[20] W. F. Egelhof, Jr., Crit. Rev. Solid State Mater. Sci. **16**, 213 (1990).

[21] B. K. Teo, *EXAFS, Basic Principles and Data Analysis* (Springer-Verlag, Berlin, 1986).

[22] P. Wetzel, C. Pirri, P. Paki, J. C. Peruchetti, D. Bolmont, and G. Gewinner, Solid State Commun. **82**, 235 (1992).

[23] V. Ghetta, E. Houssay, A. Raoult, R. Madar, and B. Lambert, C. R. Acad. Sci. Paris B **309**, 995 (1989).

[24] J. Mustre de Leon, J. J. Rehr, C. R. Natoli, C. S. Fadley, and J. Osterwalder, Phys. Rev. B **39**, 5632 (1989).

[25] A. P. Kaduwela, D. J. Friedman, and C. S. Fadley, J. Electron Spectrosc. **57**, 223 (1991).

[26] G. Gewinner, U. Kafader, P. Wetzel, and C. Pirri, J. Electron. Spectrosc. Relat. Phenom. (to be published).

[27] A. Michalovicz, *Logiciels pour la Chimie* (Société Française de Chimie, Paris, 1991), p. 402.

[28] M. H. Tuilier, C. Pirri, P. Wetzel, G. Gewinner, J. Y. Veuillen, and T. A. Nguyen Tan, Surf. Sci. **307-309**, 710 (1994).

[29] J. Stöhr, in *X-ray Absorption: Principles, Applications and Techniques of EXAFS, SEXAFS and XANES,* edited by D. C. Koningsberger and R. Prins (Wiley, New York, 1988), p. 443.

[30] D. B. B. Lollman, T. A. Nguyen Tan, J. Y. Veuillen, P. Muret, K. Leftki, M. Brunel, and J. C. Dupuy, Appl. Surf. Sci. **65/66**, 704 (1993).

[31] L. Stauffer, A. Mharchi, C. Pirri, P. Wetzel, D. Bolmont, G. Gewinner, and C. Minot, Phys. Rev. B **47**, 10 555 (1993).

[32] J. P. LaFemina, Surf. Sci. Rep. **16**, 133 (1992).

[33] J. E. Northrup, Phys. Rev. Lett. **57**, 154 (1986).

[34] J. E. Northrup, Phys. Rev. Lett. **53**, 683 (1984).

[35] J. Rubio, F. Illas, and J. M. Ricart, Phys. Rev. B **38**, 10 700 (1988).

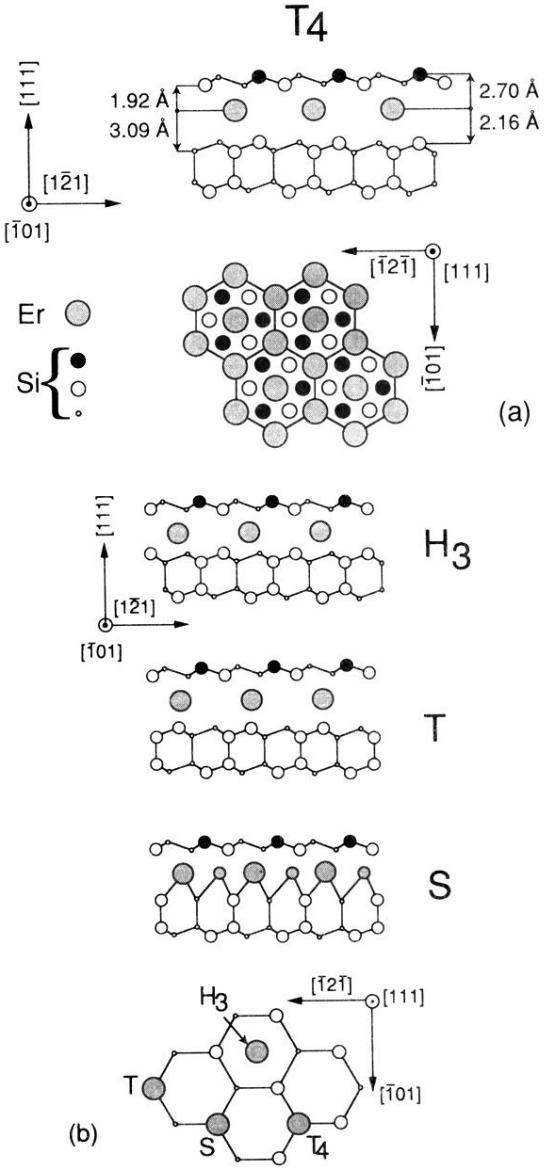

FIG. 2. (a) Top and side views of the atomic structure of a single $ErSi_2$ layer epitaxially grown on Si(111), with the optimized parameters deduced from this work. The Er is found to reside in relaxed T_4 sites, i.e., eclipsed threefold hollows of the substrate. (b) Other possible atomic geometries at the interface namely substitutional (S), top (T), and threefold hollow (H_3) tested in this work.